CMS Physics Analysis Summary

Contact: cms-pag-conveners-exotica@cern.ch

Search for long-lived particles using delayed jets and missing transverse momentum with proton-proton collisions at $\sqrt{s}$ = 13 TeV

The CMS Collaboration

Abstract

A search for long-lived particles decaying to delayed jets and missing transverse momentum is presented. The analysis is performed using a data set of 137 fb^{-1} of $\sqrt{s} = 13$ TeV proton-proton collisions recorded by the CMS experiment. Candidate signal events containing delayed jets are identified using the timing capabilities of the CMS Electromagnetic Calorimeter. The results of the search are consistent with the background prediction and are interpreted using a gauge-mediated supersymmetry breaking reference model. Masses up to 2500 and 2150 GeV are excluded for proper decay lengths of 1 m and 30 m respectively.

1 Introduction

In many beyond standard model (SM) theories the production of long-lived particles at the CERN LHC that can decay into final states containing jets and momentum imbalance ($\vec{p}_{\mathrm{T}}^{\,\mathrm{miss}}$) is predicted. Such theories include, but are not limited to, Split Supersymmetry [1, 2], SUSY with gauge-mediated supersymmetry breaking (GMSB) [3], "stealth SUSY" [4] and "Hidden Valley" models [5].

The timing capabilities of the CMS Electromagnetic Calorimeter (ECAL) are used to identify delayed jets produced by the decays of long-lived particles. This analysis is sensitive to models of new physics containing a long-lived particle which decays to a displaced jet. A representative GMSB signal model is used to benchmark the sensitivity of the search. This model contains pairs of long-lived gluinos that each decay into a gluon, which forms a jet, and a weakly interacting gravitino, which escapes the detector, causing significant $\vec{p}_{\mathrm{T}}^{\,\mathrm{miss}}$ in the event. The production diagram for the benchmark model is shown in Figure 1.

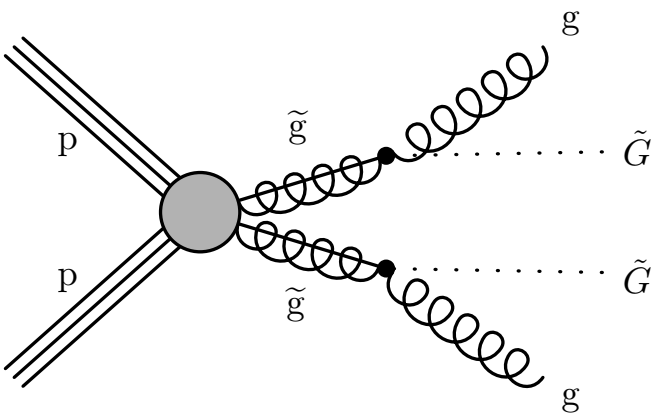

Figure 1: Feynman diagram for the gluino GMSB signal model.

There have been multiple searches for long-lived particles decaying to all-jet final-states at CMS and ATLAS at $\sqrt{s} = 8$ TeV and $\sqrt{s} = 13$ TeV [6–18]. The use of calorimeter timing has been limited to searches targeting displaced photons at $\sqrt{s} = 8$ TeV [19, 20]. This search presents the first application of ECAL timing to searching for displaced jets from long-lived particles. This technique allows the rejection of backgrounds to the few event level with high signal model efficiency with only a single displaced jet in the event. As detailed in Reference [21], such an approach allows significant new sensitivity to long-lived particle models.

This document is organized as follows. Section 2 describes the CMS apparatus. Section 3 details the reconstruction techniques for physics objects used in the analysis. Section 4 outlines the data sets used and the various software packages used to generate the samples of simulated events. Section 5 summarizes the selection criteria used to identify and categorize signal events and samples of control data. Section 6 describes the methods used to estimate the background contributions to the signal region. The results and interpretations are described in Sections 7 and 8, respectively, and summarized in Section 9.

2 The CMS detector

The central feature of the CMS detector is a superconducting solenoid of 6 m internal diameter, providing a magnetic field of 3.8 T. Within the solenoid volume are a silicon pixel and strip

tracker, a lead tungstate crystal electromagnetic calorimeter (ECAL), and a brass and scintillator hadron calorimeter (HCAL), each composed of a barrel and two endcap sections. Forward calorimeters extend the pseudorapidity coverage provided by the barrel and endcap detectors. The barrel muon system is composed of drift-tubes (DT) and resistive plate chambers (RPC). These provide high resolution hit timing and positioning to determine the muon trajectory. In the forward region the DTs are replaced by cathode strip chambers (CSC) which have greater resistance to the higher radiation flux occurring along the beamline. A more detailed description of the CMS detector, together with a definition of the coordinate system used and the relevant kinematical variables, can be found in Ref. [22].

This analysis relies on the timing capabilities of the barrel region of the ECAL [23]. The ECAL measures the energy of incoming electromagnetic particles through the scintillation light produced in the lead tungstate crystals. Silicon avalanche photodiodes (APDs) are used as photodetectors in the barrel region. These are capable of measuring the time of incoming particles with a resolution of down to $\sim (200)$ ps for energy deposits above 50 GeV [24]. Each ECAL crystal plus APD unit is referred to as an ECAL cell.

Events of interest are selected using a two-tiered trigger system [25]. The first level, composed of custom hardware processors, uses information from the calorimeters and muon detectors to select events at a rate of around 100 kHz within a time interval of less than 4 μs. The second level, known as the high-level trigger (HLT), consists of a farm of processors running a version of the full event reconstruction software optimized for fast processing, and reduces the event rate to less than 1 kHz before data storage.

3 Object and event reconstruction

The primary physics object used in this analysis are jets defined as sets of calorimeter energy deposits clustered by the anti-k_T jet clustering algorithm [26, 27] with a distance parameter of 0.4. Jets reconstructed using the Particle Flow algorithm [28] are not used in this analysis due to the non-standard tracker contribution in delayed jets. Tracks which are identified as originating from a primary vertex are associated to the jets through a requirement of $\Delta R = \sqrt{(\Delta\eta)^2 + (\Delta\phi)^2} < 0.4$, where $\Delta\eta$ and $\Delta\phi$ represent the difference between the jet axis and track in pseudorapidity and the azimuthal direction respectively.

The jet timing is determined using all ECAL cells which satisfy $\Delta R < 0.4$ between the jet and cell position and which satisfy an energy threshold of 0.5 GeV. The ECAL cell time is calibrated across the detector such that a particle travelling from the origin at (0,0,0) to the cell position at c arrives at 0 ns. Crystals with an ECAL time > 20 ns are not considered in order to reject deposits from collisions of previous or following bunches. The time of the jet, t_{jet}, is defined by the median cell time. The jet cleaning selections used to reject the dominant backgrounds are detailed in Section 5.

The estimator of the $\vec{p}_{\text{T}}^{\text{miss}}$ used for this analysis is defined as the projection on the plane perpendicular to the beams of the negative vector sum of the energies of all calorimeter energy deposits in an event (with no rejection of out-of-time ECAL cells). Its magnitude is referred to as $p_{\text{T}}^{\text{miss}}$.

4 Data sets and simulated samples

The data sample was collected in 2016, 2017, and 2018 by the CMS detector in pp collisions at a centre-of-mass energy of 13 TeV, corresponding to an integrated luminosity of 137 $\pm$

3.3 fb^{-1} [29–31]. The events must satisfy the trigger requirement of $p_{\mathrm{T}}^{\mathrm{miss}}$ (trigger) $> 120\,\text{GeV}$.

The search is interpreted using the GMSB signal model with samples produced with gluino masses from 1000 to 3000 GeV and a proper decay length ($c\tau_0$) varying from 0.3 to 30 m. All signal samples are produced with PYTHIA 8.212 [32], and NNPDF3.1LO [33] is used for PDF modeling. When a gluino or top squark is long lived, it will have enough time to form a hadronic state, an R-hadron [34, 35], which is simulated with PYTHIA. For underlying event modeling the CP2 tune is used [36].

The modeling of the jet-based cleaning variables discussed in Section 5 is validated using a simulated sample of jets produced through the strong interaction, referred to as quantum chromodynamics (QCD) multijet events. This sample is simulated with the MADGRAPH5_aMC@NLO 2.2.2 [37] event generator at leading-order (LO) accuracy. This is interfaced with PYTHIA 8.212 for parton showering, hadronisation and fragmentation. The jets from the matrix element calculations are matched to parton shower jets using the MLM algorithm [37]. The underlying event is modeled using the CUETP8M1 (CP5) tune [36] for simulation with NNPDF3.0NLO (NNPDF3.1NNLO) [33] used for PDF modeling for the 2016 (2017 and 2018) conditions.

The description of the detector response is implemented using the GEANT4 [38] package for all simulated processes. The interaction of R-hadrons with the detector is simulated [39] and found to have a negligible effect on this analysis. To model the effect of additional pp interactions within the same or nearby bunch crossings (in-time and out-of-time pileup), all simulated events are generated with a nominal distribution of pp interactions per bunch crossing and then weighted to match the pileup distribution as measured in data.

5 Event and object selection

In order to motivate the selections described in this section the various dominant sources of background expected in a search for delayed jets are detailed below.

ECAL time resolution tails Each ECAL cell time measurement has a resolution due to factors including intercalibration uncertainties, scintillator rise time differences, cell damages due to radiation, luminous region spread in z, and run-by-run variations [24].

Electronic noise Electronic noise in the ECAL can cause individual cells to record deposits with any time value, typically with low energies and uncorrelated with surrounding towers.

Direct APD hits If the ECAL cell APD is hit directly an out-of-time signal can be observed due to skipping the scintillation stage ($\approx$ 11 ns early). Such signatures can be delayed if the direct APD hit is due to a secondary interaction produced in HCAL or if the direct APD hit is from the following bunch crossing.

In-time pileup Additional pp collisions in the same bunch crossing can cause small variations in the timing due to the luminous region spread in z up to a few hundred ps.

Out-of-time pileup Additional pp collisions in the neighbouring bunch crossings can cause deposits delayed by integer multiples of the bunch spacing (25ns).

Satellite bunches The LHC radiofrequency (RF) cavities operate at a frequency of 400 MHz, such that RF 'buckets' are separated by $\approx$ 2.5 ns. In order to achieve the desired bunch spacing, only one in 10 of these buckets (separated by 25 ns) should be filled. However,

during filling a small number of protons ($\mathcal{O}(10^{-5})$ smaller than the main bunch) can be placed in adjacent 'satellite' bunches.

Beam halo Collisions between beam protons and an up-stream collimator can result in muons which pass through the detector parallel to the beam line. These "beam halo" muons may deposit energy within the ECAL causing an early signal if the beam halo is from the current or previous bunch or a delayed signal if the beam halo originates from a following bunch. The deposits due to collisions of these satellite bunches or from associated beam halo can be delayed or early relative to a main bunch collision.

Cosmic muon hits Energy deposits in the ECAL originating from cosmic muons cause out-of-time deposits which may have any time.

The events considered in this analysis are required to satisfy a series of selections to define a sample of signal events labelled as the signal region (SR). These selections are inverted to enhance particular background processes in order to predict the background contribution to the SR as detailed in Section 6.

5.1 Jet selection

5.1.1 Baseline selections

All jets considered in this analysis must pass baseline selections on the transverse momentum and pseudorapidity. A requirement of $p_{\mathrm{T}} > 30$ GeV is made to exclude contributions from pileup jets and jet axis $|\eta| < 1.48$ such that the jets are reconstructed in the ECAL barrel. The barrel selection is made as the timing resolution is significantly better in this region compared to the endcap [24], and the targeted signal model jets are strongly peaked in the central η region.

5.1.2 Cleaning selections

Jets from signal events can be expected to have a reasonably large number of ECAL cells ($N_{\mathrm{ECAL}}^{\mathrm{cell}}$) hits while jets dominated by direct APD hits or ECAL noise often have a low number of ECAL hits. A threshold of $N_{\mathrm{ECAL}}^{\mathrm{cell}} > 25$ is applied to reject these backgrounds.

Jets from signal events will on average have an approximately equal proportion of energy from ECAL and HCAL deposits while jets originating from noise or beam halo typically have a small or zero HCAL component. In order to reject such backgrounds, jets are required to satisfy $\mathrm{HEF} = E_{\mathrm{HCAL}}/(E_{\mathrm{ECAL}} + E_{\mathrm{HCAL}}) > 0.2$. An additional requirement is made of $E_{\mathrm{HCAL}} > 50\,\mathrm{GeV}$ to reject backgrounds from noise and beam halo as well as to ensure a well measured hadronic component.

Signal jets typically have a small RMS in time ($t_{\mathrm{jet}}^{\mathrm{RMS}}$) relative to their time as all the component cells originate from the same delayed jet. Jets which are significantly delayed due to uncorrelated noise are often widely spread in time values due to a small number of noise deposits coinciding with a prompt jet. In such cases the $t_{\mathrm{jet}}^{\mathrm{RMS}}$ will be correlated with t_{jet} and so backgrounds are rejected by applying a selection of both $t_{\mathrm{jet}}^{\mathrm{RMS}} < 0.4 \times t_{\mathrm{jet}}$ and on the absolute value of $t_{\mathrm{jet}}^{\mathrm{RMS}} < 2.5$ ns. For jets with $|t_{\mathrm{jet}}| < 3$ns the selection is made on $t_{\mathrm{jet}}^{\mathrm{RMS}} < 0.4 \times 3 = 1.2$ ns.

Jets which originate from the primary vertex (PV) and have a mismeasured time or originate from satellite bunch collisions typically contain a large number of tracks associated to the PV. The $PV_{\mathrm{track}}^{\mathrm{fraction}}$, defined as the ratio of the total momentum of all PV tracks associated to the jet to the transverse energy, is used to identify signal jets which do not originate from the PV. A selection of $PV_{\mathrm{track}}^{\mathrm{fraction}} < 1/12$ is applied.

Beam halo muons will travel directly through the Cathode Strip Chamber (CSC) muon detector before leaving energy deposits in the ECAL, so the fraction of ECAL energy that can be associated to CSC segments provides direct rejection of backgrounds from beam halo. The ratio of the total energy of ECAL cells matched to a CSC segment ($\Delta\phi < 0.04$) to E_{ECAL}, defined as $E^{\mathrm{CSC}}_{\mathrm{ECAL}}/E_{\mathrm{ECAL}}$, is used to discriminate beam halo backgrounds. A selection of $E^{\mathrm{CSC}}_{\mathrm{ECAL}}/E_{\mathrm{ECAL}} < 0.8$ is applied.

5.2 Event selection

A selection on the missing transverse momentum of $p_{\mathrm{T}}^{\mathrm{miss}} > 300$ GeV is applied to reject backgrounds from multijet production (including collisions from satellite bunches).

The DT and RPC muon systems are used to veto backgrounds from cosmic ray muons. The signal models may also cause deposits in the muon systems if the jets contain muons, there is 'punch-through' of hadronic energy to the muon system, or if a long-lived particle decays within the muon systems. To mitigate the inefficiency for the signal models, only the DT segments and RPC hits with $r > 560$ cm (where r is the transverse radial distance to the interaction point) and RPC stations with $|z| > 600$ cm (where z is the distance along the beamline to the interaction point) are considered. In order to reduce the effect of noise, DT segments and RPC hits are required to be within $\Delta R < 0.5$ of a DT segment with a hit. The maximal $\Delta\phi$ between such 'paired' DT segments and RPC hits is defined as $\max(\Delta\phi^{DT_{ij}}_{\mathrm{paired}})$ and $\max(\Delta\phi^{RPC_{ij}}_{\mathrm{paired}})$ respectively. Events satisfying $\max(\Delta\phi^{DT_{ij}}_{\mathrm{paired}}) > \pi/2$ or $\max(\Delta\phi^{RPC_{ij}}_{\mathrm{paired}}) > \pi/2$ are rejected to veto cosmic muon events.

Finally, events are required to satisfy a series of filters designed to ensure the reconstruction is of good quality and to contain at least one jet satisfying the requirements outlined in Section 5.1. These selections are summarised in Table 1.

6 Background estimation

This section details the characterisation of the dominant background sources and the prediction methods used to estimate residual contributions to the signal region. The backgrounds are investigated by inverting the selections on the discriminating variables summarised in Table 1 to define control regions enriched in particular background processes.

There are three main background sources which are predicted separately: beam halo backgrounds which typically have low HEF and large $E^{\mathrm{CSC}}_{\mathrm{ECAL}}/E_{\mathrm{ECAL}}$, out-of-time backgrounds from satellite bunch collisions which have large $PV^{\mathrm{fraction}}_{\mathrm{track}}$, and jets originating from cosmic muons which have high $\max(\Delta\phi^{DT/RPC_{ij}}_{\mathrm{paired}})$ and $t^{\mathrm{RMS}}_{\mathrm{jet}}$.

The backgrounds are predicted from the control regions using methods which rely on data. The data from all three years are combined in making these predictions due to the low number of events in the signal region phase space. These predictions are tested using validation regions which do not overlap with the signal regions to ensure the prediction is unbiased. The closure in the validation region is used to define a systematic uncertainty on the prediction in the signal region.

6.1 Beam halo

The beam halo contribution is predicted by measuring the pass/fail ratio of the selection $E^{\mathrm{CSC}}_{\mathrm{ECAL}}/E_{\mathrm{ECAL}} > 0.8$ for events with HEF < 0.2 and applying it to the observed number of

Table 1: Summary of the selections used to define the signal region.

Event level selections	
Event level	$p_{\mathrm{T}}^{\mathrm{miss}} > 300$ GeV
Event level	Quality filters
Event level	$\max(\Delta\phi_{\mathrm{paired}}^{DT_{ij}}) < \pi/2$
Event level	$\max(\Delta\phi_{\mathrm{paired}}^{RPC_{ij}}) < \pi/2$
Jet baseline selections	
Jet	$\lvert\eta\rvert < 1.48$
Jet	$p_{\mathrm{T}} > 30$ GeV
Jet cleaning selections	
Jet	$E_{\mathrm{ECAL}} > 20$ GeV
Jet	$N_{\mathrm{ECAL}}^{\mathrm{cell}} > 25$
Jet	HEF > 0.2 AND $E_{\mathrm{HCAL}} > 50$ GeV
Jet	$(t_{\mathrm{jet}}^{\mathrm{RMS}}/t_{\mathrm{jet}} < 0.4$ AND $t_{\mathrm{jet}}^{\mathrm{RMS}} < 2.5)$ OR $t_{\mathrm{jet}}^{\mathrm{RMS}} < 1.2$
Jet	$PV_{\mathrm{track}}^{\mathrm{fraction}} < 1/12$
Jet	$E_{\mathrm{ECAL}}^{\mathrm{CSC}}/E_{\mathrm{ECAL}} < 0.8$
Jet	$t_{\mathrm{jet}} > 3$ ns

events with HEF > 0.2. The signal region prediction is made using all events with $t_{\mathrm{jet}} > 3$ ns. The prediction is made without any selection on E_{HCAL} and is therefore a conservative estimate.

To ensure that this prediction is unbiased, a validation region is defined by selecting events with $t_{\mathrm{jet}} < -3$ ns and passing all signal selections except those on $E_{\mathrm{ECAL}}^{\mathrm{CSC}}/E_{\mathrm{ECAL}}$, HEF, and E_{HCAL}. To enhance the contribution of beam halo events relative to the contributions from satellite bunches and cosmic muons in the validation region, the ϕ value of the jets is required to be within 0.2 radians of 0 or $\pm\pi$.

The correlation between $E_{\mathrm{ECAL}}^{\mathrm{CSC}}/E_{\mathrm{ECAL}}$ and HEF in the validation sample is consistent with zero, meaning they can be used to form an unbiased prediction. The prediction from this method for the number of events passing signal thresholds on $E_{\mathrm{ECAL}}^{\mathrm{CSC}}/E_{\mathrm{ECAL}}$ and HEF in the validation region is $0.02^{+0.06}_{-0.02}$, in agreement with the 0 events observed.

The closure in the validation region is used to derive an additional systematic uncertainty on the prediction. The gradient of a linear fit to the pass/fail ratio of the $E_{\mathrm{ECAL}}^{\mathrm{CSC}}/E_{\mathrm{ECAL}} > 0.8$ selection as a function of HEF is found to be consistent with zero. The uncertainty is then propagated to the observed event counts with $E_{\mathrm{ECAL}}^{\mathrm{CSC}}/E_{\mathrm{ECAL}} > 0.8$ and HEF > 0.2. The final prediction for the signal region is $0.02^{+0.06}_{-0.02}\,(\mathrm{stat})\,^{+0.05}_{-0.01}\,(\mathrm{syst})$.

6.2 Core and satellite collision background prediction

The core and satellite collision contribution is predicted by measuring the pass/fail ratio of the selection $PV_{\text{track}}^{\text{fraction}} < 1/12$ for events with $1 < t_{\text{jet}} < 3$ and applying it to the observed number of events with $t_{\text{jet}} > 3\,\text{ns}$ and $PV_{\text{track}}^{\text{fraction}} > 1/12$. Two validation regions are defined to verify the prediction of the satellite bunch and timing tail backgrounds.

The first validation region is selected to contain events with $t_{\text{jet}} < -1$ ns and passing all signal selections except for that on $PV_{\text{track}}^{\text{fraction}}$. The pass/fail ratio of the $PV_{\text{track}}^{\text{fraction}} < 1/12$ selection is measured for events with $-3\,\text{ns} < t_{\text{jet}} < -1\,\text{ns}$ and applied to the number of events with $t_{\text{jet}} < -3\,\text{ns}$ and $PV_{\text{track}}^{\text{fraction}} > 1/12$. The upper bound on t_{jet} ensures the sample is enriched with jets in the tail of the t_{jet} distribution. The correlation between the variables in the validation region is confirmed to be consistent with zero, which allows an unbiased prediction to be made. The prediction from this method for the number of events passing $t_{\text{jet}} < -3\,\text{ns}$ and $PV_{\text{track}}^{\text{fraction}} < 1/12$ is $0.09^{+0.2}_{-0.06}$ and the number of events observed is 1. The event passing selection has no paired RPC or DT hits and is therefore unlikely to originate from a cosmic. This is compatible with expectation, but as the tension is slightly more than one sigma, a further validation is carried out. The selection of $p_{\text{T}}^{\text{miss}} > 300\,\text{GeV}$ is inverted and the prediction repeated. In this region 1.95 ± 0.29 events are predicted and 1 event is observed. The observation in the negative time region for $p_{\text{T}}^{\text{miss}} > 300\,\text{GeV}$ is therefore concluded to be consistent with an upwards fluctuation.

A second validation region is defined using events with $1\,\text{ns} < t_{\text{jet}} < 3\,\text{ns}$. The pass/fail ratio of the $PV_{\text{track}}^{\text{fraction}} < 1/12$ selection is measured for events with $1\,\text{ns} < t_{\text{jet}} < 2\,\text{ns}$ and applied to the number of events with $2\,\text{ns} < t_{\text{jet}} < 3\,\text{ns}$ and $PV_{\text{track}}^{\text{fraction}} > 1/12$. The t_{jet} and $PV_{\text{track}}^{\text{fraction}}$ variables are uncorrelated meaning they can provide an unbiased prediction. The prediction from this method for the number of events passing $t_{\text{jet}} > 2$ ns and $PV_{\text{track}}^{\text{fraction}} < 1/12$ is $0.03^{+0.08}_{-0.03}$, in agreement with the 0 events observed.

The prediction for the signal region relies on using the efficiency of the $PV_{\text{track}}^{\text{fraction}}$ selection of events with $1 < t_{\text{jet}} < 3$ ns to predict the efficiency of the $PV_{\text{track}}^{\text{fraction}}$ selection for $t_{\text{jet}} > 3$ ns. Due to differences in the reconstruction of the calorimeter energy and tracker p_{T} this efficiency may be expected to have some small time dependence. In order to measure any such t_{jet} dependence and derive an associated systematic uncertainty, a data sample with the offline $p_{\text{T}}^{\text{miss}}$ selection inverted (but passing trigger requirements) and $t_{\text{jet}} > 2$ ns is used. The region of $PV_{\text{track}}^{\text{fraction}} < 1/12$ is not included to avoid contamination from cosmic or beam halo muon deposits. The gradient of a linear fit to the pass/fail ratio of a looser selection of $PV_{\text{track}}^{\text{fraction}} < 0.5$ against t_{jet} is consistent with zero. Similarly to the case for the beam halo prediction, the uncertainty is propagated to the observed event counts with $t_{\text{jet}} > 3\,\text{ns}$ and $PV_{\text{track}}^{\text{fraction}} > 1/12$. The final prediction for the satellite and core background is $0.11^{+0.09}_{-0.05}\,(\text{stat})\,^{+0.02}_{-0.02}\,(\text{syst})$ events.

6.3 Cosmic events

The discriminating variables used for the cosmic prediction are the $t_{\text{jet}}^{\text{RMS}}$ of the jet and the maximum of $\max(\Delta\phi_{\text{paired}}^{DT_{ij}})$ and $\max(\Delta\phi_{\text{paired}}^{RPC_{ij}})$, labelled as $\max(\Delta\phi_{\text{paired}}^{DT/RPC_{ij}})$. The pass/fail ratio of the $t_{\text{jet}}^{\text{RMS}} < 2.5\,\text{ns}$ selection is measured for events with $\max(\Delta\phi_{\text{paired}}^{DT/RPC_{ij}}) > \pi/2$ and applied to events with $\max(\Delta\phi_{\text{paired}}^{DT/RPC_{ij}}) < \pi/2$. Cosmic muons passing through the HCAL will typically only deposit significant energy in a single isolated cell. The HCAL noise rejection quality filters are designed to veto events containing such isolated deposits and so inverting these filters, with all other selections applied, provides a validation region enriched in events

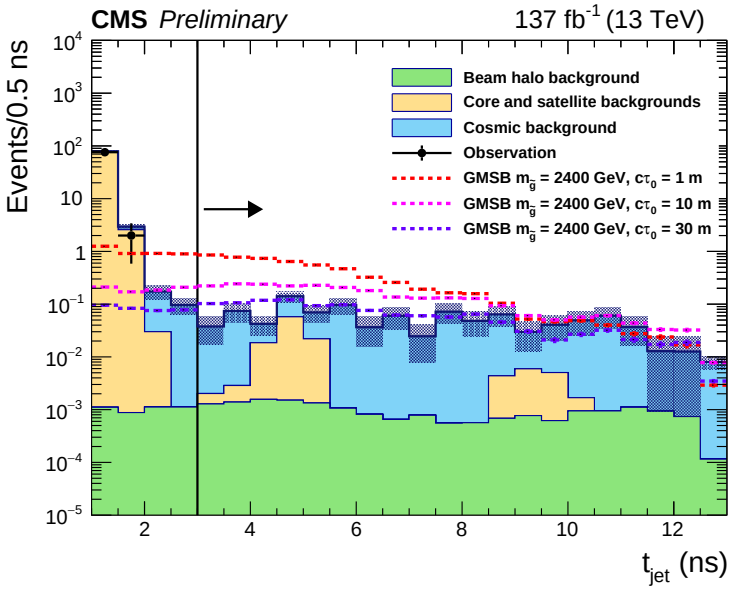

Figure 2: The timing distribution of the backgrounds predicted to contribute to the signal region is compared to representative signal models. The templates for the major backgrounds are taken from control regions and normalised by the predictions detailed in Section 6. No events are observed in data for $t_{\text{jet}} > 3\,\text{ns}$.

with cosmic muons.

The correlation between $t_{\text{jet}}^{\text{RMS}}$ and $\max(\Delta\phi_{\text{paired}}^{DT/RPC_{ij}})$ in the validation sample is consistent with zero, meaning they can be used to form an unbiased prediction. The prediction in the validation region for the number of events passing signal thresholds on $t_{\text{jet}}^{\text{RMS}}$ and $\max(\Delta\phi_{\text{paired}}^{DT/RPC_{ij}})$ is $1.1^{+1.9}_{-1.1}$, in agreement with the 1 event observed. An additional systematic uncertainty is applied from the statistical power of the validation region. The final prediction in the signal region is $1.0^{+1.8}_{-1.0}\,(\text{stat})\,^{+1.8}_{-1.0}\,(\text{syst})$

6.4 Background summary

The predicted background yields are summarised in Table 2. The overall background prediction is $1^{+2.5}_{-1}$ events.

Table 2: Background prediction summary.

Background	Prediction
Beam halo	$0.02^{+0.06}_{-0.02}\,(\text{stat})\,^{+0.05}_{-0.01}\,(\text{syst})$
Core and satellite bunches	$0.11^{+0.09}_{-0.05}\,(\text{stat})\,^{+0.02}_{-0.02}\,(\text{syst})$
Cosmics	$1.0^{+1.8}_{-1.0}\,(\text{stat})\,^{+1.8}_{-1.0}\,(\text{syst})$

7 Results

Figure 2 shows the timing distribution for events with jets passing all signal region selections. The templates are for illustration purposes only and are not used for the statistical interpretation. The overall prediction for the signal region is $1^{+2.5}_{-1}$ events which is consistent with the observation of 0 events.

8 Interpretation

The model used for the interpretation is the GMSB SUSY model in which gluinos are pair produced and form R-hadrons. The long-lived gluinos then decay to a gluon and gravitino producing a delayed jet and missing energy. The experimental acceptance times efficiency ($\mathcal{A}\varepsilon$), shown in Figure 3, is evaluated independently for each model point, defined in terms of gluino mass ($m_{\tilde{g}}$) and lifetime ($c\tau_0$). The efficiency is maximised for high gluino masses and for a range in $c\tau_0$, bounded by the requirements that the gluino must have sufficient lifetime for its decay products to pass the $t_{\text{jet}} > 3$ ns selection and that the gluino must decay before or within the ECAL. For a gluino model with $m_{\tilde{g}} = 2000$ GeV the efficiency is maximal for the range $1 < c\tau_0 < 10$ m. The efficiency is maximised for higher masses due to the increased $p_{\text{T}}^{\text{miss}}$ in the event and smaller β of the gluino.

The trigger efficiency for the simulated samples is evaluated from the trigger emulation. The inefficiency due to the $p_{\text{T}}^{\text{miss}}$ trigger requirement ranges from $\sim 5\%$ to $\sim 15\%$ for $c\tau_0 = 1$ and 10 m respectively.

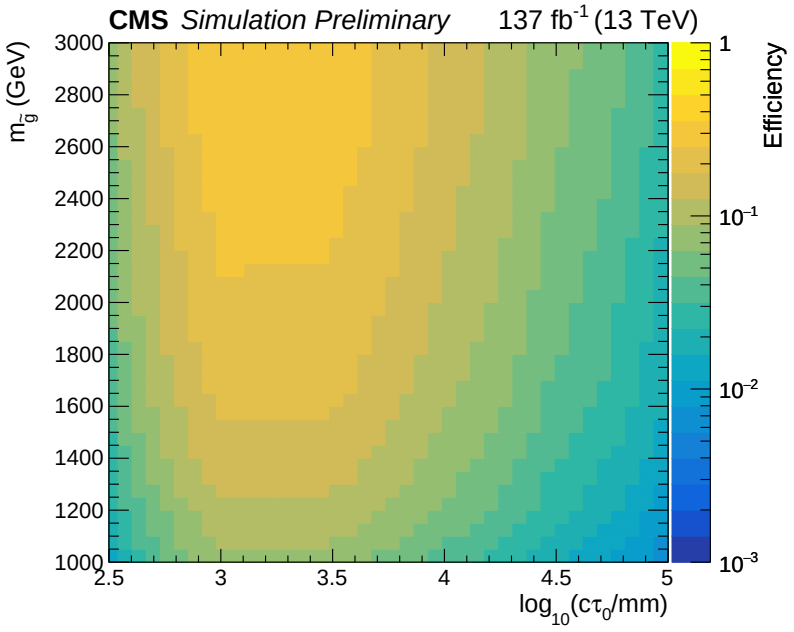

Figure 3: Efficiency in the mass and $c\tau_0$ plane for the GMSB model after all selections.

In order to evaluate systematic uncertainties in the modeling of the jet variables discussed in Section 5.1.2 the distributions for multijet simulation are compared to data. For each jet variable, the threshold used for the selection is varied in the simulation to match the efficiency measured in data. The change in acceptance from this variation is shown for each of the cleaning variables in Table 3 using an example model point. This variation is taken as a system-

atic uncertainty on the signal model acceptance. The variation on $t_{\text{jet}}^{\text{RMS}}$ is also propagated to $t_{\text{jet}}^{\text{RMS}}/t_{\text{jet}}$.

Table 3: The derived variation on the acceptance on the modelling of the jet variables discussed in Section 5.1.2 for a representative model with $m_{\tilde{g}} = 2400$ GeV.

Variable	Derived uncertainty (%)	
	$m_{\tilde{g}} = 2400$ GeV, $c\tau_0 = 1$ m	$m_{\tilde{g}} = 2400$ GeV, $c\tau_0 = 10$ m
$PV_{\text{track}}^{\text{fraction}}$	0.01	0.03
$N_{\text{ECAL}}^{\text{cell}}$	3.2	4.2
HEF	2.8	2.5
$E_{\text{ECAL}}^{\text{CSC}}/E_{\text{ECAL}}$	0.9	0.9
$t_{\text{jet}}^{\text{RMS}}$	22	15

In addition to the uncertainty on the modelling of the jet cleaning variables the systematic uncertainties on the signal $\mathcal{A}\varepsilon$ are summarised below.

- Modelling of dedicated cleaning variables (detailed in Section 5.1.2): typical size documented in Table 3, taken as correlated between years.
- Luminosity: 2.5%, 2.3%, 2.5% uncertainty in 2016, 2017, and 2018, taken as uncorrelated between years.
- Trigger: size of inefficiency taken as systematic variation, taken as correlated between years.
- Limited simulated sample statistics: few % depending on signal model acceptance, uncorrelated between years.
- Pileup reweighting: 4.6% uncertainty on the minimum bias cross section, taken as correlated between years.
- Jet energy resolution/scale: few % uncertainty on the signal region acceptance.

Under the signal+background hypothesis a modified frequentist approach is used to determine observed upper limits (σ_{UL}) at 95% confidence level (CL) on the cross section (σ) times branching ratio (BR) squared for producing a pair of gluinos, each decaying to a gluon and gravitino, as a function of $m_{\tilde{g}}$ and $c\tau_0$. The approach is based on the profile likelihood ratio as the test statistic [40] and the CL_s criterion [41, 42]. The σ_{UL} is evaluated through the use of pseudo-data sets. Potential signal contributions to event counts in both the signal and control regions are considered.

Figure 4 shows the observed σ_{UL} as a function of lifetime and gluino mass for the GMSB model. Gluino masses of up to 2100, 2500, and 2150 GeV are excluded for $c\tau_0 = 0.3$, 1.0, and 30 m respectively. The dependence of the expected and observed σ_{UL} as a function of $c\tau_0$ is shown in Figure 5 for $m_{\tilde{g}} = 2400$ GeV. The observed limit is compared to the results of the CMS displaced jet search [43], highlighting the complementary coverage.

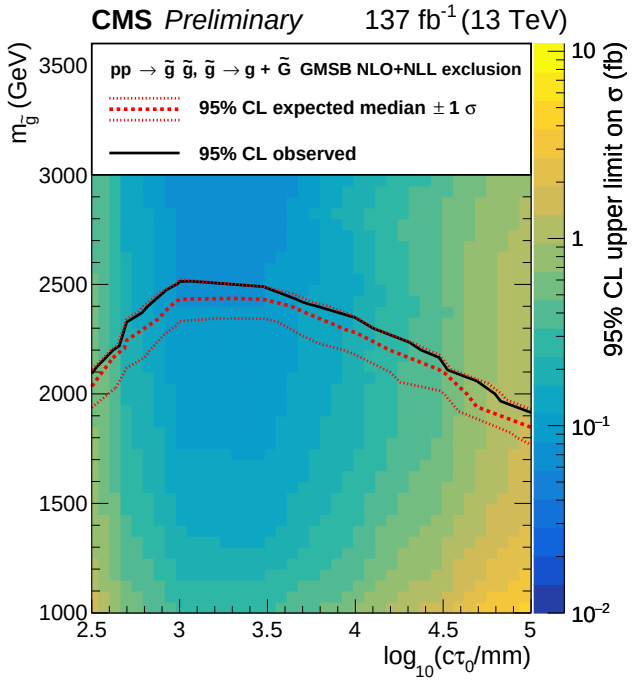

Figure 4: The 95% CL observed upper limits on $\sigma \times \mathrm{BR}^2$ in the mass and $c\tau_0$ plane for the GMSB model after all selections for 137 fb^{-1}. The contour of 95% CL expected upper limits on $\sigma/\sigma_{\text{theory}} = 1$ is shown in the solid line while the plus and minus one sigma variations are shown in the dashed lines. The observed limit is shown in the solid black line.

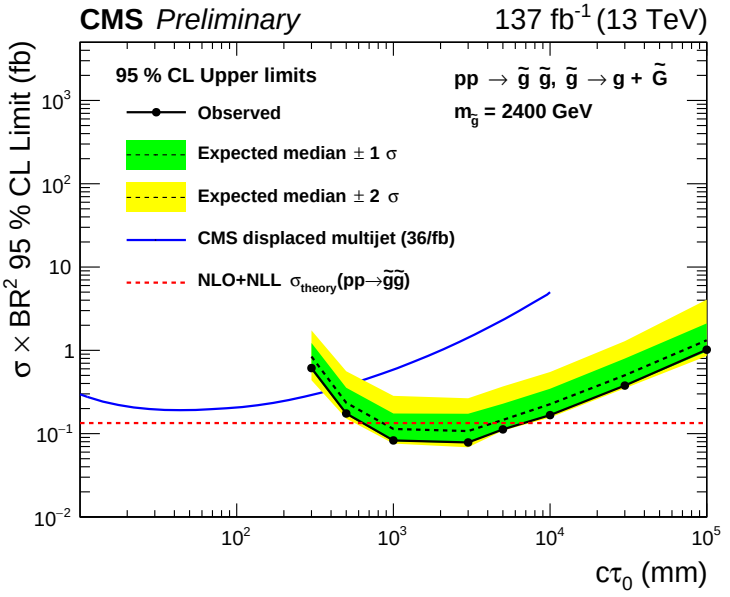

(a)

Figure 5: Expected and observed limit on $\sigma \times \mathrm{BR}^2$ after all signal region selections for a gluino GMSB model with $m_{\tilde{g}} = 2400$ GeV are shown in the dotted and solid black lines respectively. The one (two) sigma variation in the expected limit is shown in green (yellow). The blue solid line shows the observed limit achieved by the CMS displaced jet search [43].

9 Summary

An inclusive search for long-lived particles is reported, based on a data sample of pp collisions collected at $\sqrt{s} = 13\,\text{TeV}$, corresponding to an integrated luminosity of 137 fb^{-1}. The search uses timing of electromagnetic energy deposits to select delayed jets from the decays from heavy long-lived particles, with residual backgrounds estimated using measurements in control regions of the data. The results are interpreted using the gluino GMSB signal model, and gluino masses below 2100 GeV are excluded for decay lengths of ctau between 0.3 and 30 m. The reach is significantly extended in comparison to tracker based searches at CMS and ATLAS for $c\tau_0 > \sim 1\,\text{m}$ [16, 43, 44].

References

[1] N. Arkani-Hamed and S. Dimopoulos, "Supersymmetric unification without low energy supersymmetry and signatures for fine-tuning at the LHC", *JHEP* **06** (2005) 073, doi:10.1088/1126-6708/2005/06/073, arXiv:hep-th/0405159.

[2] G. F. Giudice and A. Romanino, "Split supersymmetry", *Nucl. Phys. B* **699** (2004) 65, doi:10.1016/j.nuclphysb.2004.08.001, arXiv:hep-ph/0406088. [Erratum: doi:10.1016/j.nuclphysb.2004.11.048].

[3] Z. Liu and B. Tweedie, "The Fate of Long-Lived Superparticles with Hadronic Decays after LHC Run 1", *JHEP* **06** (2015) 042, doi:10.1007/JHEP06(2015)042, arXiv:1503.05923.

[4] J. Fan, M. Reece, and J. T. Ruderman, "Stealth Supersymmetry", *JHEP* **11** (2011) 012, doi:10.1007/JHEP11(2011)012, arXiv:1105.5135.

[5] M. J. Strassler and K. M. Zurek, "Echoes of a hidden valley at hadron colliders", *Physics Letters B* **651** (2007), no. 5, 374, doi:https://doi.org/10.1016/j.physletb.2007.06.055.

[6] CMS Collaboration, "Search for stopped gluinos in p p collisions at $\sqrt{s} = 7$ TeV", *Phys. Rev. Lett.* **106** (2011) 011801, doi:10.1103/PhysRevLett.106.011801, arXiv:1011.5861.

[7] CMS Collaboration, "Search for heavy stable charged particles in pp collisions at $\sqrt{s} = 7$ TeV", *JHEP* **03** (2011) 024, doi:10.1007/JHEP03(2011)024, arXiv:1101.1645.

[8] ATLAS Collaboration, "Search for stable hadronising squarks and gluinos with the ATLAS experiment at the LHC", *Phys. Lett. B* **701** (2011) 1, doi:10.1016/j.physletb.2011.05.010, arXiv:1103.1984.

[9] ATLAS Collaboration, "Search for decays of stopped, long-lived particles from 7 TeV p p collisions with the ATLAS detector", *Eur. Phys. J. C* **72** (2012) 1965, doi:10.1140/epjc/s10052-012-1965-6, arXiv:1201.5595.

[10] CMS Collaboration, "Search for heavy long-lived charged particles in pp collisions at $\sqrt{s} = 7$ TeV", *Phys. Lett. B* **713** (2012) 408, doi:10.1016/j.physletb.2012.06.023, arXiv:1205.0272.

[11] ATLAS Collaboration, "Search for long-lived stopped R-hadrons decaying out-of-time with p p collisions using the ATLAS detector", *Phys. Rev. D* **88** (2013) 112003, doi:10.1103/PhysRevD.88.112003, arXiv:1310.6584.

[12] CMS Collaboration, "Search for decays of stopped long-lived particles produced in proton-proton collisions at $\sqrt{s} = 8$ TeV", *Eur. Phys. J. C* **75** (2015) 151, doi:10.1140/epjc/s10052-015-3367-z, arXiv:1501.05603.

[13] ATLAS Collaboration, "Search for massive, long-lived particles using multitrack displaced vertices or displaced lepton pairs in p p collisions at $\sqrt{s} = 8$ TeV with the ATLAS detector", *Phys. Rev. D* **92** (2015) 072004, doi:10.1103/PhysRevD.92.072004, arXiv:1504.05162.

[14] ATLAS Collaboration, "Search for metastable heavy charged particles with large ionization energy loss in p p collisions at $\sqrt{s} = 13$ TeV using the ATLAS experiment", *Phys. Rev. D* **93** (2016) 112015, doi:10.1103/PhysRevD.93.112015, arXiv:1604.04520.

[15] CMS Collaboration, "Search for long-lived charged particles in proton-proton collisions at $\sqrt{s} = 13$ TeV", *Phys. Rev. D* **94** (2016) 112004, doi:10.1103/PhysRevD.94.112004, arXiv:1609.08382.

[16] ATLAS Collaboration, "Search for long-lived, massive particles in events with displaced vertices and missing transverse momentum in $\sqrt{s}$ = 13 TeV pp collisions with the ATLAS detector", *Phys. Rev.* **D97** (2018) 052012, doi:10.1103/PhysRevD.97.052012, arXiv:1710.04901.

[17] CMS Collaboration, "Search for decays of stopped exotic long-lived particles produced in proton-proton collisions at 13 TeV", *Journal of High Energy Physics* **2018** (May, 2018) 127, doi:10.1007/JHEP05(2018)127.

[18] ATLAS Collaboration, "Search for long-lived neutral particles in pp collisions at $\sqrt{s}$ = 13 TeV that decay into displaced hadronic jets in the ATLAS calorimeter", arXiv:1902.03094.

[19] CMS Collaboration, "Search for long-lived particles in events with photons and missing energy in proton-proton collisions at $\sqrt{s} = 7$ tev", *Physics Letters B* **722** (2013) 273, doi:https://doi.org/10.1016/j.physletb.2013.04.027.

[20] ATLAS Collaboration, "Search for nonpointing and delayed photons in the diphoton and missing transverse momentum final state in 8 TeV pp collisions at the LHC using the ATLAS detector", *Phys. Rev.* **D90** (2014), no. 11, 112005, doi:10.1103/PhysRevD.90.112005, arXiv:1409.5542.

[21] J. Liu, Z. Liu, and L.-T. Wang, "Long-lived particles at the LHC: catching them in time", arXiv:1805.05957.

[22] CMS Collaboration, "The CMS experiment at the CERN LHC", *JINST* **3** (2008) S08004, doi:10.1088/1748-0221/3/08/S08004.

[23] CMS Collaboration, "The CMS electromagnetic calorimeter project: Technical Design Report", technical report, CERN, Geneva, 1997.

[24] D. del Re, "Timing performance of the CMS ECAL and prospects for the future", *Journal of Physics: Conference Series* **587** (2015), no. 1, 012003.

[25] CMS Collaboration, "The CMS trigger system", *JINST* **12** (2017) P01020, doi:10.1088/1748-0221/12/01/P01020, arXiv:1609.02366.

[26] M. Cacciari, G. P. Salam, and G. Soyez, "The Anti-k(t) jet clustering algorithm", *JHEP* **0804** (2008) 063, doi:10.1088/1126-6708/2008/04/063, arXiv:0802.1189.

[27] M. Cacciari, G. P. Salam, and G. Soyez, "FastJet User Manual", *Eur. Phys. J.* **C72** (2012) 1896, doi:10.1140/epjc/s10052-012-1896-2, arXiv:1111.6097.

[28] CMS Collaboration, "Particle-flow reconstruction and global event description with the CMS detector", *JINST* **12** (2017) P10003, doi:10.1088/1748-0221/12/10/P10003, arXiv:1706.04965.

[29] CMS Collaboration, "CMS Luminosity Measurements for the 2016 Data Taking Period", Technical Report CMS-PAS-LUM-17-001, CERN, Geneva, 2017.

[30] CMS Collaboration, "CMS luminosity measurement for the 2017 data-taking period at $\sqrt{s} = 13$ TeV", Technical Report CMS-PAS-LUM-17-004, CERN, Geneva, 2018.

[31] CMS Collaboration, "CMS luminosity measurement for the 2018 data-taking period at $\sqrt{s} = 13$ TeV", Technical Report CMS-PAS-LUM-18-002, CERN, Geneva, 2018.

[32] T. Sjostrand, S. Mrenna, and P. Z. Skands, "A Brief Introduction to PYTHIA 8.1", *Comput. Phys. Commun.* **178** (2008) 852–867, doi:10.1016/j.cpc.2008.01.036, arXiv:0710.3820.

[33] NNPDF Collaboration, "Parton distributions for the LHC Run II", *JHEP* **04** (2015) 040, doi:10.1007/JHEP04(2015)040, arXiv:1410.8849.

[34] M. Fairbairn et al., "Stable massive particles at colliders", *Phys. Rept.* **438** (2007) 1, doi:10.1016/j.physrep.2006.10.002, arXiv:hep-ph/0611040.

[35] A. C. Kraan, "Interactions of heavy stable hadronizing particles", *Eur. Phys. J. C* **37** (2004) 91, doi:10.1140/epjc/s2004-01946-6, arXiv:hep-ex/0404001.

[36] CMS Collaboration, "Extraction and validation of a new set of CMS PYTHIA8 tunes from underlying-event measurements", Technical Report CMS-PAS-GEN-17-001, CERN, Geneva, 2018.

[37] J. Alwall et al., "The automated computation of tree-level and next-to-leading order differential cross sections, and their matching to parton shower simulations", *JHEP* **07** (2014) 079, doi:10.1007/JHEP07(2014)079, arXiv:1405.0301.

[38] GEANT4 Collaboration, "GEANT4—a simulation toolkit", *Nucl. Instr. Meth. A* **506** (2003) 250, doi:10.1016/S0168-9002(03)01368-8.

[39] R. Mackeprang and D. A. Milstead, "An updated description of heavy-hadron interactions in geant-4", *The European Physical Journal C* **66** (Apr, 2010) 493, doi:10.1140/epjc/s10052-010-1262-1.

[40] ATLAS Collaboration and CMS Collaboration, "Procedure for the LHC Higgs boson search combination in Summer 2011", Technical Report CMS-NOTE-2011-005. ATL-PHYS-PUB-2011-11, CERN, 2011.

[41] T. Junk, "Confidence level computation for combining searches with small statistics", *Nucl. Instr. Meth. A* **434** (1999) 435, doi:10.1016/S0168-9002(99)00498-2, arXiv:hep-ex/9902006.

[42] A. L. Read, "Presentation of search results: the CL_s technique", *J. Phys. G* **28** (2002) 2693, doi:10.1088/0954-3899/28/10/313.

[43] CMS Collaboration, "Search for long-lived particles with displaced vertices in multijet events in proton-proton collisions at $\sqrt{s}$ =13 TeV", *Phys. Rev.* **D98** (2018) 092011, doi:10.1103/PhysRevD.98.092011, arXiv:1808.03078.

[44] CMS Collaboration, "Search for long-lived particles decaying into displaced jets in proton-proton collisions at $\sqrt{s} = 13$ TeV", *Submitted to: Phys. Rev.* (2018) arXiv:1811.07991.